N O T I C E

THIS DOCUMENT HAS BEEN REPRODUCED FROM MICROFICHE. ALTHOUGH IT IS RECOGNIZED THAT CERTAIN PORTIONS ARE ILLEGIBLE, IT IS BEING RELEASED IN THE INTEREST OF MAKING AVAILABLE AS MUCH INFORMATION AS POSSIBLE

NASA

# Technical Memorandum 82153



# Determination of Rain Rate from a Spaceborne Radar Using Measurements of Total Attenuation

Robert Meneghini
Jerome Eckerman
David Atlas



JUNE 1981

National Aeronautics and
Space Administration

**Goddard Space Flight Center**
Greenbelt, Maryland 20771

## ABSTRACT

Several experimental and theoretical studies have shown that path-integrated rain rates can be determined by means of a direct measurement of attenuation. For ground based radars this is done by measuring the backscattering cross section of a fixed target in the presence and absence of rain along the radar beam. A ratio of the two measurements yields a factor proportional to the attenuation from which the average rain rate can be deduced. In this paper, we extend the technique to spaceborne radars by choosing the ground as reference target. The technique is also generalized so that both the average and range-profiled rain rates can be determined. The accuracies of the resulting estimates are evaluated for a narrow beam radar located on a low earth orbiting satellite.

TABLE OF CONTENTS

INTRODUCTION ..... 1

THE SURFACE REFERENCE TECHNIQUE ..... 3

RANGE PROFILING OF THE RAIN RATE ..... 6

RESULTS AND DISCUSSION ..... 10

CONCLUSIONS ..... 18

REFERENCES ..... 20

APPENDIX ..... 23

# DETERMINATION OF RAIN RATE FROM A SPACEBORNE RADAR USING MEASUREMENTS OF TOTAL ATTENUATION

## INTRODUCTION

Radar is the most promising spaceborne instrument for quantitative measurements of rainfall rate over land. For this application, however, radars that operate at non-attenuating wavelengths have several disadvantages. The restrictions on antenna size from space preclude fields of view small enough at the longer wavelengths to resolve the more intense regions of rain rate. As the resolution requirements are relaxed, the partially filled range cells lead to errors caused by spatial averaging, small signal to noise ratios, and reflectivity gradients. Apart from the errors caused by poor resolution, the Z-R law (used in deriving the rain rate R from the reflectivity factor Z) is a sensitive function of the unknown drop size distribution (DSD) [1]. When conditioned on a knowledge of the synoptic storm conditions, some of the large scale variability in the DSD can be eliminated; nevertheless, a significant variability persists within each class of storm [2]. The resulting errors, along with typical calibration errors of 2db to 3db limit the accuracy of rain rate determination from a single non-attenuating wavelength radar.

While short wavelength attenuating radars offer better resolution for a fixed antenna size, the measurement accuracy of R is degraded not only by errors in the calibration constant and the Z-R relationship but also by errors in the attenuation coefficient-rain rate law (k-R). As in the Z-R law, a major source of error in the k-R law arises from systematic changes in the DSD as well as fluctuations in the DSD within each storm class. For moderate to large values of attenuation, even small errors in the k-R relationship can introduce a large bias into the rain rate estimate [3].

The addition of an independent measurement of some meteorological quantity can often reduce one or more of the errors mentioned above. One of the first examples of this type of correction procedure was given by Hitschfeld and Bordan [3]. These authors proposed an independent measurement of rain rate at some point along the radar beam which served to bound the errors in the rain rate estimate. The dual-wavelength methods [4-6] can also be viewed as a type of correction procedure in which the measurements are used to derive a two parameter DSD. The liquid

water content and the rain rate can then be deduced without the need of Z-R or k-R laws. Other dual measurement techniques include the use of orthogonal polarizations [7,8] and the use of a combined radar-radiometric sensor [9].

Of particular importance for the work presented here is the method [10-14] in which a direct measurement of total attenuation is used to find the path-integrated or the path-averaged rain rate. The attenuation is obtained from a ratio of the backscattered powers from a fixed target where one measurement is made in the presence, the other in the absence of precipitation. From the attenuation, an appropriate k-R law, and the path length from the radar to the target, the path-integrated or average rain rate can be determined without recourse to the Z-R law or the radar calibration constant. Atlas and Ulbrich [14] have shown, moreover, that at wavelengths near 0.86 cm., the k-R law is essentially independent of the DSD. This independence is manifested in less scatter about the k-R regression line and therefore a reduction in the error variance of R.

For satellite applications, the technique is not directly applicable because of the impracticability of a global network of calibrated targets. The objectives of this paper are twofold: to modify the technique to make it suitable for spaceborne radars and to generalize it so that, in addition to the average rain rate, range-profiled rain rates can be estimated.

## THE SURFACE REFERENCE TECHNIQUE

By means of an attenuating-wavelength spaceborne radar, measurements of the backscattering coefficient (i.e. the scattering cross section per unit area) of the surface, $\sigma^o$, can be made in the rain-free areas adjacent to the rain volume. As the beam passes into regions of precipitation, the backscattered power from the surface will be proportional to $\sigma^o A$ where A is the attenuation factor. If the incidence angle and the radar frequency can be chosen so that the values of $\sigma^o$ within and outside the precipitation are nearly invariant, then the ratio of the two measurements yields an accurate estimate of A. Once A has been obtained the average rain rate follows from a k-R law and a measurement of the path length through the rain [15].

In the standard methods, $\sigma^o$ is obtained from a measurement made in the absence of precipitation. In the present technique, which we will refer to as a surface reference technique (SRT), the actual $\sigma^o$ is an unknown which can be approximated either by an average value $\bar{\sigma}^o$ measured in the rain-free areas adjacent to the target or by a subsequent measurement of $\sigma^o$ at the actual target when precipitation along the radar beam is absent. The replacement of the actual with an 'equivalent' reference measurement introduces an additional error into the determination of rain rate, the magnitude of which depends on the spatial or temporal inhomogeneity of the surface scattering properties.

To restate the above ideas in a more quantitative manner, we let $P_{R_j}$ denote the radar return power from the rain at the jth range bin. We further classify the surface return according to whether precipitation is present or absent along the radar beam, choosing $P'_{G_j}$ as the surface return in the presence of precipitation and $P_{G_j}$ as the unattenuated surface return. In the subsequent discussions we will often have need to distinguish between those range bins (within the main beam) which intercept the surface from those which do not. We refer to the former as surface bins and the latter as precipitation bins as shown in Fig. 1.

As shown in the appendix the return powers at the nth range bin can be approximated by

$$P_{G_n} = C_G \, \sigma_1^o / r_n^3 \tag{1}$$

$$P'_{G_n} = C_G \, \sigma_2^{\circ} \, A_n / r_n^3 \tag{2}$$

where

$$A_n \approx e^{-0.46 \int_{r_o}^{r_n} k \, ds} \tag{3}$$

k is the attenuation coefficient in db/km, $C_G$ is a calibration constant, $r_o$ is the distance from the radar to the edge of the storm, and $r_n$ is the range corresponding to the center of the nth range bin. The subscripts on $\sigma^{\circ}$ are used to indicate that the values of $\sigma^{\circ}$ for the two measurements are generally different. The ratio of $P'_{G_n}$ to $P_{G_n}$ then provides an estimate of $A_n$. In general, however, the return power from the surface cell, n, in the presence of precipitation will include a contribution from this precipitation (see Fig. 1). If we also account for the noise power, $P_N$, added to the return by the receiver, then the estimate of $A_n$, written $\hat{A}_n$, is given by the ratio of the total return powers measured at the surface bin n in the presence and absence of precipitation:

$$\hat{A}_n = P_{1n} / P_{2n} \tag{4}$$

where

$$P_{1n} = P'_{G_n} + P_{R_n} + P_{N_1} \tag{5}$$

$$P_{2_n} = P_{G_n} + P_{N_2} \tag{6}$$

The subscripts added to $P_N$ indicate that these contributions are not constant over the two measurements.

Using the k-R law, $k=\gamma R^{\xi}$, in (3) and the estimated value $P_{1n}/P_{2n}$ above for $A_n$, then,

$$\int_{r_o}^{r_n} R^{\xi} \, ds = - \frac{1}{0.46 \, \gamma} \, \ell n \, (P_{1n}/P_{2n}) \tag{7}$$

Defining the average rain rate to be

$$R_{AV} = \frac{1}{r_e} \int_{r_o}^{r_n} R \, ds \tag{8}$$

with

$$r_e = r_n - r_o \tag{9}$$

we notice that for an arbitrary spatial distribution of rain rate along the beam and $\xi \neq 1$, $R_{Av}$ can not be expressed in terms of $P_{1n}$, $P_{2n}$. Instead, we approximate the average rain rate by

$$\left( \frac{1}{r_e} \int_{r_o}^{r_n} R^{\xi} ds \right)^{1/\xi}$$

so that upon using (7), the estimated rain rate can be written in terms of the measured quantities $P_{1n}$, $P_{2n}$, $r_e$ and the assumed values $\gamma$, $\xi$ by

$$\hat{R}_{AV} = \left[ -\frac{1}{0.46 \gamma r_e} \ln (P_{1n}/P_{2n}) \right]^{1/\xi} \tag{10}$$

For wavelengths between 0.7 cm and 2 cm we can use the approximation $\xi = 1$ and adjust $\gamma$ accordingly without a great deal of increase in the variance in the k-R law [14].

## RANGE PROFILING OF THE RAIN RATE

To obtain profiled rain rates (i.e. rain rates at each range bin) we can begin either with the Hitschfeld-Bordan algorithm [3] or the iterative algorithms proposed by Ormsby [16]. Although these techniques themselves provide range profiled rain rates, they are susceptible to large errors whenever the total attenuation is significant. Since the SRT is feasible only when moderate to large attenuations occur, the above methods are of limited applicability in this instance. We can, however, reformulate them by using the total attenuation, obtained from the SRT, to bound the errors in the rain rate. In fact, the procedure to be described is similar to the Hitschfeld-Bordan correction technique mentioned above except that the attenuation estimate of (4) now takes the place of the independent measurement of rain rate.

For the particular application used here, the Hitschfeld-Bordan algorithm has been shown to yield better results than the iterative estimates. We therefore deal exclusively with the former. The Hitschfeld-Bordan algorithm for the rainfall rate at the jth range bin can be written [17],

$$R_j^{H-B} = a\, Z_{m_j}^{b} \left( 1 - 0.46\, \alpha \beta\, h \sum_{i=1}^{j} \epsilon_i\, Z_{m_i}^{\beta} \right)^{-b/\beta} \tag{11}$$

with

$$\epsilon_i = \begin{cases} 1 & i \neq j \\ 1/2 & i = j \end{cases}$$

The reflectivity factor $Z_j$, the measured reflectivity factor $Z_{m_j}$ and the calibration constant $C_R$ are related by the equations

$$Z_{m_j} = A_j\, Z_j \tag{12}$$

$$Z_{m_j} = r_j^2\, P_{R_j}/C_R \tag{13}$$

where $r_j$, $P_{R_j}$, $A_j$ have been defined previously. Using the k-Z law, $k = \alpha Z^{\beta}$ and (3) then

$$A_j = e^{-0.46\, \alpha \int_{r_o}^{r_j} Z^{\beta}(s)\, ds} \tag{14}$$

Equation (11) follows from the Z-R relationship, $R = aZ^b$, equation (12) and the fact that

$$A_j^{\beta} = \left(1 - 0.46\,\alpha\beta\,h \sum_{i=1}^{j} \epsilon_i\, Z_{m_i}{}^{\beta}\right) \tag{15}$$

which is a consequence of (12) and (14). The quantity h in (11) and (15) is the radar range resolution which arises in approximating an integral by a summation, i.e.,

$$\int_{r_o}^{r_j} Z^{\beta}(s)\,ds \approx h \sum_{i=1}^{j} \epsilon_i\, Z_i{}^{\beta} \quad .$$

We now assume that an estimate of the attenuation factor up to the nth range bin, $\hat{A}_n$, is available. There are several ways of incorporating this additional measurement into the rain rate estimate of (11). We discuss two possibilities.

Case 1: To account for an offset in the calibration constant $C_R$, we multiply the set $\{Z_{m_i}\}$, $i = 1, 2, \ldots, j$ in (11) by some constant, say p. Since $Z_{m_j} = P_{R_j}\, r_j{}^2 / C_R$, this operation is equivalent to multiplying $C_R$ by $p^{-1}$. Equation (11) then becomes

$$\hat{R}_j^{H\text{-}B} = a\,(p\,Z_{m_j})^b \left(1 - 0.46\,\alpha\beta\,h \sum_{i=1}^{j} \epsilon_i\,(p\,Z_{m_i})^{\beta}\right)^{-b/\beta} \quad . \tag{16}$$

Identifying $pZ_{m_i}$ as a corrected form of $Z_{m_i}$, then from (15),

$$A_j = \left[1 - 0.46\,\alpha\beta\,h \sum_{i=1}^{j} \epsilon_i\,(p\,Z_{m_i})^{\beta}\right]^{-b/\beta} \quad .$$

Letting j increase to n in this formula, using for $A_n$ the estimated value $\hat{A}_n$ from (4), and solving for p gives

$$p = \left[(1 - \hat{A}_n{}^{\beta}) \,/\, 0.46\,\alpha\beta\,h \sum_{i=1}^{n} \epsilon_i\, Z_{m_i}^{\beta}\right]^{1/\beta}$$

The quantity p is now inserted back into (16) which yields a new rain rate estimate that we label with a superscript 1:

$$\hat{R}_j^{(1)} = a Z_{m_j}^{\ b} J \left(1 - (1 - \hat{A}_n^{\ \beta}) S_j / S_n\right)^{-b/\beta} \tag{17}$$

where

$$J = \left((1 - \hat{A}_n^{\ \beta}) / 0.46 \alpha \beta \overline{h S_n}\right)^{b/\beta} \tag{18}$$

$$S_j = \sum_{i=1}^{j} \epsilon_i Z_{m_i}^{\ \beta} \tag{19}$$

These equations are valid for $j = 1, ..., n$. Equation (17) can be interpreted as an alternative form of the Hitschfeld-Bordan algorithm in which the quantity $\hat{A}_n$ has been used to eliminate offset errors in the radar calibration constant, $C_R$.

Case 2: To compensate for offset errors in $\alpha$, where $k = \alpha Z^{\beta}$, we replace $\alpha$ by $\alpha p'$ in (11) and (15). Proceeding in the same way as in Case 1, we find

$$p' = (1 - \hat{A}_n^{\ \beta}) / 0.46 \alpha \beta S_n$$

The quantity $p'$, in turn, yields a second rain rate estimate, $R_j^{(2)}$, that can be written

$$\hat{R}_j^{(2)} = a Z_{m_j}^{\ b} (1 - (1 - \hat{A}_n^{\ \beta}) S_j / S_n)^{-b/\beta} \tag{20}$$

for $j \leq n$.

Although the only difference between (17) and (20) is the factor of J appearing in the former, it can be seen upon inspection that (20) is independent of offsets in $\alpha$ but dependent on errors in the calibration constant. Exactly the opposite is true of (17).

In both cases considered the total attenuation, as determined by the SRT, was used to derive a parameter which provides a bound to the Hitschfeld-Bordan algorithm thereby eliminating the occurance of extremely large errors. It is worthwhile noting that a number of other range profiled rain rate estimates can be deduced. For example, if the path integrated rain rate, $R_p$, is defined to be $\int_{r_0}^{r_n} R \, ds$, then from (7) an estimate of this quantity is,

$$\hat{R}_p = \left[\int_{r_0}^{r_n} R^{\eta} \, ds\right]^{1/\eta} = \left[\frac{1}{0.46 \gamma} \ln \hat{A}_n\right]^{1/\eta} \tag{21}$$

On the other hand, $\hat{R}_p$ can be estimated from any of the following quantities:

$$h \sum_{1}^{n} \hat{R}_j^{H\text{-}B} ,$$

$$h \sum_{1}^{n} \hat{R}_j^{(1)} ,$$

$$h \sum_{1}^{n} \hat{R}_j^{(2)} ,$$

where $\hat{R}^{H\text{-}B}$, $\hat{R}^{(1)}$, $\hat{R}^{(2)}$ are given by (11), (17), and (20) respectively.

If we multiply by some constant certain variables in any of these three quantities and adjust it until an equality with (21) is obtained, the constants found in this way supply new estimates of range profiled rain rate. In this paper only the estimates given by (10), (17), and (20) will be analyzed. An analysis of the other estimates would probably be warranted only after an experimental verification of the basic technique.

## RESULTS AND DISCUSSION

The remainder of the paper will be spent in investigating the behavior of equations (10), (17) and (20) in the context of a down-looking radar located on a low earth orbiting platform. In particular, we compute the mean and standard deviation of $\hat{R}_{AV}$, $\hat{R}^{(1)}$, $\hat{R}^{(2)}$ as functions of rain rate for suitable values of transmit power, wavelength, antenna diameter, etc. The parameters that will be kept constant are listed in table 1. Since the quality of the $\hat{R}^{(1)}$, $\hat{R}^{(2)}$ estimates varies markedly with distance into the storm, their statistics are presented as a function of range.

The procedure for finding the statistics of the above estimates can be conveniently described as a two-stage process. In the first stage, the average values of the return power from the rain and the surface are computed as a function of distance into the storm (see appendix). The second stage in this procedure is to introduce offset errors and random variations into several of the radar and meteorological quantities. Via a simulation, these quantities are used to compute particular realizations of $\hat{R}_{AV}$, $\hat{R}^{(1)}$ and $\hat{R}^{(2)}$ in accordance with equations (10), (17), and (20). Continuing in this way over one thousand such realizations, we then compute the sample mean and standard deviation of $\hat{R}_{AV}$ and of $\hat{R}^{(1)}$, $\hat{R}^{(2)}$ for $j = 1, \ldots, n$ where $j = 1$ corresponds to the first bin containing rain at the storm top while $j = n$ corresponds to the bin at which the surface return power is maximum.

An example of the mean power calculation is shown in figure 2 where the receiver noise power, $P_N$ (N), the rain return, $P_R$ (R), and the surface or clutter return, $P'_G$ (C) have been plotted at each range bin. The abscissa represents the slant range which is measured from the storm top downward into the rain. Several features of the plot are worth noticing. In the first several range bins the rain return power increases because of the progressively greater fractional volume filled with precipitation. After the peak rain return has been reached, corresponding to the first fully filled bin, it begins decreasing with a slope proportional to the attenuation factor. This behavior continues until the range bin of the main lobe intercepts the surface; thereafter, the rain return falls off more rapidly because of the smaller volume of rain contributing to the backscattered power. The surface clutter follows a somewhat reversed progression. This contribution arises from the annulus formed by the intersection of concentric spheres with a flat earth. As the radar pulse

propagates through the storm, the annulus expands until a portion of it intersects the main lobe. This intersection corresponds to the broad maximum of the ground return shown in the figure.

To describe the sources of error in the rain rate estimates, we first note that in (17) and (20) the measured reflectivity factor at the jth bin, $Z_{m_j}$, was defined to be

$$Z_{m_j} = P_{R_j} r_j^2 / C_R$$

However, the rain return from the jth bin, $P_{R_j}$, is not a measured quantity but rather the total return power from that bin, $P_{1_j}$. We can also account for possible calibration errors by writing $C_R = \overline{C}_R (1 + \epsilon_R)$ where $\epsilon_R$ is the relative error in $C_R$ and $\overline{C}_R$ is the true value. Defining $\hat{Z}_{m_j}$ as the estimated value of $Z_{m_j}$, then

$$\hat{Z}_{m_j} = P_{1_j} r_j^2 / \overline{C}_R (1 + \epsilon_R) \tag{22}$$

where $P_{1_j}$ is given by (5); i.e.,

$$P_{1_j} = P_{R_j} + P_{G_j} + P_{N_1}$$

In computing the statistics of $\hat{R}^{(1)}$, $\hat{R}^{(2)}$, $\hat{Z}_{m_j}$ is replaced everywhere in (17) and (20) by $\hat{Z}_{m_j}$.

To characterize the errors in the return power from the precipitation, we write

$$P_R = \overline{P}_R \, f(K) \tag{23}$$

where $\overline{P}_R$ is the mean value of $P_R$ which is given by equation (A4). f(K) is a random variable of mean 1 and variance 1/K, where K is the effective number of independent samples [18-20]. If we stipulate that the radar is to provide contiguous coverage, then for the fairly high spatial resolution that will be considered, K is usually too small to guarantee an accurate measurement of $P_R$. Several strategies are available, however, to increase K which include: pulse compression [21], the broad-band radar [22], frequency agility and multiple beams. An evaluation of these various schemes is beyond the scope of this paper. We assume for simplicity that a sufficiently large K is achieved by the use of multiple beams. The total peak transmitted power then becomes $mP_T$ where m is the number of beams and $P_T$ is the peak transmitted power per beam.

In a similar manner, the receiver noise power, $P_N$, is written

$$P_N = \bar{P}_N \, f(K') \tag{24}$$

where K' is the total number of samples per range bin (assuming that all samples of the noise power are independent) and where

$$\bar{P}_N \cong k_\beta \, T \, B \, F$$

where $k_\beta$ is Boltzmann's constant, T is the receiver temperature in degrees Kelvin, F is the noise figure of the receiver, and B is the receiver bandwidth. We have chosen T = 290°K, F = 5 db, and B = $1/\tau$ (where $\tau$ is the pulse duration) throughout.

The return powers from the bround, $P'_{G_j}$, $P_{G_j}$ are proportional to the backscattering coefficients $\sigma_1{}^\circ$, $\sigma_2{}^\circ$, respectively. In general $\sigma^\circ$ is a function of wavelength, incidence angle, and polarization of the incident wave. In the context of the simulation, $\sigma_1{}^\circ$, $\sigma_2{}^\circ$ are chosen to be independent and identically distributed log-normal random variables. The mean of $\sigma^\circ$ is taken from the vegetation model of Ulaby [23] who has fit the extensive Kansas data to an eight parameter equation. The results of the simulation are presented for several values for the standard deviation of $\sigma^\circ$, written $S_o$, which are: $S_o$ = 0.9, 1.8, 2.7 db. The value $S_o$ = 1.8 db corresponds approximately with that given by Ulaby. For all examples, we have chosen the incident wave to be horizontally polarized.

Substituting (22) and (23) into (21) then

$$\hat{Z}_{m_j} = P_{1_j} \, r_j^2 / \bar{C}_R \, (1 + \epsilon_R) \tag{25}$$

where

$$P_{1_j} = \bar{P}_{R_j} \, f(K) + P'_{G_j} + \bar{P}_N \, f(K') \tag{26}$$

The random variables f(K), f(K'), and $P'_{G_j}$ are assumed to be mutually independent.

The estimate of the attenuation factor is found from (4) where $P_{1_n}$ is given by (25) with n replacing j and where

$$P_{2_n} = P_{G_n} + \bar{P}_N \, f_2(K') \quad . \tag{27}$$

To complete the characterization of the sources in error in $\hat{R}_{AV}$, $\hat{R}^{(1)}$, $\hat{R}^{(2)}$ we must approximate the errors arising from the use of the k-R, Z-R, and k-Z relationships in these estimates. Writing, as before,

$$k = \gamma R^{\xi}$$

$$R = a Z^{b}$$

$$k = \alpha Z^{\beta}$$

we make the following assumptions. In the k-R relationship, we fix $\xi$ and chose $\gamma$ to be normally distributed with an unbiased mean and standard deviation given by Atlas and Ulbrich [14]. Similarly, for the Z-R relationship we fix b and choose a to be normally distributed with an unbiased mean and a standard deviation equal to 25% of the mean value. The above relationships are not independent; therefore $\alpha,\beta$ can be expressed in terms of $\gamma,\xi,a,b$, i.e.,

$$\beta = \xi^{b} \tag{28}$$

$$\alpha = \gamma a^{\xi} \tag{29}$$

Before presenting the results, it is instructive to recognize some of the requirements that $P_R$, $P_G'$ must satisfy so that reasonably accurate measurements of $\hat{R}_{AV}$, $\hat{R}_j^{(1)}$, $\hat{R}_j^{(2)}$ can be made. Since the most critical variables in the rain rate estimates are $\hat{A}_n$ and $\hat{Z}_{m_j}$, we discuss these exclusively. To obtain $\hat{A}_n$ accurately, we must insure that at one or more of the surface bins the following inequalities hold: $P_G' >> P_N$, $P_G' >> P_R$. If these conditions are satisfied, then from (1), (2) and (4)-(6)

$$\hat{A}_n \approx P'_{G_n}/P_{G_n} = \sigma_1^{\circ}/\sigma_2^{\circ} A_n \tag{30}$$

where $A_n$ is the true attenuation factor out to the nth range bin. A second necessary condition for an accurate estimate of $A_n$ is seen immediately from (30): only if the random variables $\sigma_1^{\circ}$, $\sigma_2^{\circ}$ are close to one another in a statistical sense will $\hat{A}_n$ be an indication of the attenuation factor rather than the spatial or temporal fluctuations in $\sigma^{\circ}$. Thus, in so far as possible, the incidence angle and wavelength should be chosen so that effects such as soil moisture and surface roughness

are minimized. This can be partially realized by a selection of K-band frequencies and incident angles pointed away from nadir.

From (5), (13), (22) it follows that an accurate determination of $\hat{Z}_{m_j}$ requires that $\overline{P}_{R_j} >> \overline{P}_N$ and $\overline{P}_{R_j} >> \overline{P}'_{G_j}$, j = 1, ..., n. This second inequality, however, is in direct opposition to the above requirements that $\overline{P}'_{G_j} >> \overline{P}_R$ at one or more of the surface cells. Since the latter condition is essential to the accuracy of the method, the accuracy of $Z_{m_j}$ must be sacrificed at these surface cells. At the precipitation cells, however, the condition $\overline{P}_R >> \overline{P}'_G$ can be retained.

It is not difficult to select system parameters so that most of the above conditions are satisfied over some band of rain rates. By referring to Fig. 2, it can be seen that $\overline{P}_R >> \overline{P}_G$, $\overline{P}_R >> \overline{P}_N$ over all precipitation cells, excepting those at the storm top where a significant portion of the bin is unfilled. Furthermore, at several of the surface bins, the conditions $\overline{P}_G >> \overline{P}_R$, $\overline{P}'_G >> \overline{P}_N$ hold. We conclude that at $\lambda$ = 1.24 cm., R = 5 mm/hr and for the parameters listed in Table 1, the necessary conditions for rain rate estimation via the SRT are fulfilled.

Results of the simulation are presented in Figs. 3 through 6. Each plot gives the mean and standard deviation of $\hat{R}_{AV}$ (both normalized by the true rain rate, $R_T$) and of $\hat{R}^{(1)}$, $\hat{R}^{(2)}$ as functions of distance into the storm for a fixed values of wavelength and rain rate. In all cases, the true rain rate is assumed to be constant within the slab extending from z = 0 to z = $z_s$ and zero elsewhere. Since $\hat{R}_{AV}$ is not a function of range, we obtain single values for the normalized mean and standard deviation. In the figures, this normalized mean is represented by a horizontal line.

For example, in Fig. 3, where $\lambda$ = 1.24 cm, R = 5 mm/hr and $S_o$ = 1.8 db, the normalized mean, $\overline{R}_{AV}/R_T$, equals 0.94; that is, the estimate has a small negative bias. At the end of this line and corresponding to the nth range bin a vertical bar is plotted of magnitude equal to twice the normalized standard deviation of $\hat{R}_{AV}$, $2S_{AV}$, where $S_{AV} = \sigma_{AV}/R_T$. Again referring to Fig. 3, we can measure this length by projecting it onto the vertical scale. We find that $\sigma_{AV}$ = 1.5. The same conventions are used to display the normalized mean and standard deviation of $\hat{R}^{(1)}$, $\hat{R}^{(2)}$. In Fig. 4, for example, at r = 3 km we find that $\overline{R^{(1)}}/R_T = 0.87$, $\sigma_1/R_T = 0.07$ and $\overline{R^{(2)}}/R_T = 0.75$, $\sigma_2/R_T = 0.23$.

As an aside we note that the figures indicate that only in the mid-ranges from about 2.5 to 6.5 km (comprising about 50% of the total number of range bins) can we even attempt to adequately estimate the range-profiled rain rate. This mid-range consists of those bins in the main beam that do not intercept the ground and that are also nearly or fully filled with rain. It is easy to show that as the antenna diameter to wavelength ratio, $D/\lambda$, is increased, the number of partially filled cells decreases. For example, at $D/\lambda = 1000$, approximately 80% of the bins are relatively free from such errors. Such large values of $D/\lambda$, however, introduce problems of their own. At more modest values of $D/\lambda$, steps might be taken to estimate partial beam-filling [24] or attempt to separate, by means of Doppler processing, the surface from the rain return.

If the wavelength is fixed at $\lambda = 1.24$ cm and the rain rate is decreased below 5 mm/hr, $\bar{R}_{AV}$ soon becomes larger than the true rain rate (positively biased) while the normalized standard deviation of $\hat{R}_{AV}$ becomes progressively larger. For example, at $R = 1$ mm/hr, $\bar{R}_{AV} = 1.68$ and $\sigma_{AV} = 1.1$, indicating that the SRT is not feasible at this rain rate and wavelength. By going to rain rates larger than 5 mm/hr, the normalized standard deviation of $\hat{R}_{AV}$ is significantly reduced while accompanied by only a slight increase in negative bias. These trends continue up to about 20-25 mm/hr where the noise power, $P_N$, becomes comparable to $P'_{G_n}$. For rain rates beyond 25 mm/hr, the bias in $\hat{R}_{AV}$, $\hat{R}^{(1)}$, $\hat{R}^{(2)}$ begins to increase rapidly. Fig. 4 is plotted for the same parameters as in Fig. 3 except that $R_T = 20$ mm/hr. The increased bias and the reduction of the normalized variance with larger rain rate is evident on comparing the two figures.

If we accept as adequate those estimates with an offset and standard deviation less than 25% of the true value, then at $\lambda = 1.24$ cm, $S_o = 1.8$ db, and with the values of the radar parameters in Table 1, we find that we can estimate the average rain rate between about 7 mm/hr and 20 mm/hr. If $S_o$ is reduced to 0.9 db the minimum and maximum rain rates become 4 mm/hr and 25 mm/hr. These values and the results at two other frequencies are presented in Table 2. The main determining factor for these minimum and maximum rain rates is the magnitude of the total attenuation up to the nth range bin. When the attenuation, $\int_{r_o}^{r_n} k(s)\,ds$, is slight (low rain rates) $R_{AV}$ will

generally be greater than the true value: this is due to the logarithm in (10) which biases values of $A_n$ near unity toward the larger values of $\hat{R}_{AV}$. On the other hand, when the attenuation is large (high rain rates) the noise power, $P_N$, eventually predominates over $P'_{G_n}$, giving from (4)-(6) an attenuation factor $A_n$ larger than the true value. This leads to an underestimate of the attenuation, and therefore, an underestimate of the true average rain rate.

The statistics of $\hat{R}^{(1)}$, $\hat{R}^{(2)}$ in the mid-ranges follow the same general behavior as those of $\hat{R}_{AV}$. Notice, however, in Figs. 4 and 5 that the mean values of $\hat{R}^{(1)}$, $\hat{R}^{(2)}$ exhibit a gradual decrease from about 3 km to 6 km followed by an increase around 6.5 km which corresponds to the intersection of the range bin with the surface. Both effects can be explained by the presence of the ground clutter which leads to an overestimation of $Z_m$ as is shown by (21). This overestimation of $Z_m$ is especially large at the surface cells and implies that for $j \neq n$, the ratio $S_j/S_n$ is smaller than the true value. This, in turn, negatively biases the estimates of (17) and (20). On the other hand, as j approaches n, then $S_j/S_n \rightarrow 1$ and the greatest contributor to the bias is caused by the $Z_m^{\,b}$ factor in (17) and (20) which produces a positive bias in the rain rate estimates. These effects account for the abrupt change in the mean value at about 6.5 km from negatively to positively biased values.

Despite the similarities between $\hat{R}^{(1)}$, $\hat{R}^{(2)}$, there are several differences between them. As mentioned before, $\hat{R}^{(1)}$ is independent of errors in the calibration constant $C_R$. Thus in the usual situation where the errors in $C_R$ are 2 db or greater, $\hat{R}^{(1)}$ is preferable to $\hat{R}^{(2)}$. To show this graphically, we plot in Figs. 5 and 6 the statistics of $\hat{R}_{AV}$, $\hat{R}^{(1)}$, $\hat{R}^{(2)}$ for $R_T = 20$ mm/hr and $\lambda = 1.87$ cm. In Fig. 5 the error in $C_R$ is chosen to be zero. In Fig. 6, $C_R$ is in error by 3 db; i.e. $\epsilon_R = 2$ in (21). Notice that neither $\hat{R}_{AV}$ or $\hat{R}^{(1)}$ is affected by this offset.

Although the figures indicate that the variance in $\hat{R}^{(1)}$ is generally smaller than $\hat{R}^{(2)}$, this may be somewhat misleading because of the simplified error model used for the k-R, Z-R, k-Z relationships. In particular, we find from (27), (28) that $\gamma = \alpha\, a^{-\beta/b}$ and $\eta = \beta\, b^{-1}$ so that (17) can be written

$$\hat{R}_j^{(1)} = \hat{Z}_{m_j}^{\,b}\, J' \left(1 - (1 - \hat{A}_n^{\,\beta})\, S_j/S_n\right)^{-1/\eta}$$

where

$$J' = \left( (1 - \hat{A}_n^{\beta}) / 0.46\, \gamma\, \beta\, h\, S_n \right)^{1/\eta}.$$

In this form, $\hat{R}^{(1)}$ is no longer explicitly dependent on $\alpha$ and a. Since $\eta$, b, $\beta$ were assumed to be fixed, the only sources of variability besides $\hat{Z}_{m_j}$, $S_j$, $\hat{A}_n^{\beta}$ is in $\gamma$. To obtain a better indication of the variance in $\hat{R}_j^{(1)}$ and $\hat{R}_j^{(2)}$, a more sophisticated model is required for the characterization of errors in the k-R, Z-R, k-Z relationships.

## CONCLUSIONS

By using the surface as a reference target, the total attenuation method can be extended to spaceborne geometries. This method provides estimates of path-averaged rain rate that are independent of the Z-R law and radar calibration constant but dependent on the backscattering coefficient of the surface and the k-R relation. Range-profiled estimates of rain rate can be deduced by means of a reformulated version of the Hitschfeld-Bordan algorithm. This reformulation was done by using the total attenuation, as determined from the surface reference method, to derive a parameter which bounds the error in the original estimate. Of the two estimates that were analyzed, the $\hat{R}^{(1)}$ estimate was preferable because of its insensitivity to radar calibration errors.

To generate the results that have been presented, a simple meteorological model has been used. Although the errors caused by simple partial beam-filling effects were included, no spatial variation in the rain rate was assumed. Furthermore, the effects of atmospheric absorption, clouds and precipitation above the melting layer were neglected as was the presence of non-spherical drops. These assumptions were made to decrease computation time and to simplify the presentation of the results. Nevertheless, these effects would have to be accounted for in a more rigorous assessment of the technique.

In the modelling of the fluctuations in $\sigma^o$, i.e. the variability introduced by substituting the actual for an equivalent target, we have used in one set of calculations, a $S_o$ = 1.8 db taken from Ulaby [23]. This value, however, includes data taken over different crop types, soil conditions and times of the growing season. Since some of these sources of error will be absent in the data used for estimating the attenuation factor, we expect, on the average, to encounter lower values of $S_o$. Selected runs through Skylab data [15] taken at $\lambda$ = 2.16 cm for an incident angle of 33° have yielded a $S_o$ between adjacent 10 km footprints of about 0.43 db. The standard deviation in $\sigma^o$ from values separated by 5 to 10 instantaneous fields of view (IFOV) was found to be 0.5 to 0.6 db. These values, however, are probably too low for the type of application envisaged since the Skylab IFOV (about 4 times the area of that considered in the simulation) would tend to smooth over anomalous features appearing in the footprint. Furthermore, in the SRT, the changes in soil

moisture conditions and the presence or absence of moisture on crops, leaves, etc., would tend to make $\sigma^0$ more variable than on the average. Because of our lack of knowledge of $\sigma^0$, the simulation was carried out for three values of this quantity. The results have shown that the minimum rain rate that can be estimated accurately is a fairly sensitive function of this parameter.

One of the limitations of the surface reference technique appears to be the narrow range of rain rates over which a single frequency radar can work well. In particular, it was found that below a certain rain rate, the total attenuation is too small for the technique to work effectively. In this region of slight attenuation, however, the iterative algorithm or the Hitschfeld-Bordan algorithm works best. It appears likely that the dynamic range can be extended by using one of the standard attenuating wavelength techniques for estimation at the low rain rates. For a dual-wavelength radar, additional hybrid techniques would be available.

As a final comment we remark that the SRT has been analyzed only for rain over land. Over ocean it is expected to be less accurate because of the dependence of $\sigma^0$ on wind speed for angles greater than 10°. For measurements over ocean however, a radar-radiometer sensor might be feasible. In this mode the total attenuation would be obtained from the radiometric intensity measurement while the radar would provide a measure of the storm height and the range-profiled reflectivities. The rain rate algorithms of (17) and (20) would then be applicable to this sensor if the quantity $A_n$ were interpreted as the radiometrically-derived attenuation factor.

## REFERENCES


(1) D. Atlas and C. W. Ulbrich, "The physical basis for attenuation-rainfall relationships and the measurement of rainfall parameters by combined attenuation and radar methods", J. Rech. Atmos., vol. 8, pp. 275-298, 1974.

(2) G. E. Stout and E. A. Mueller, "Survey of relationships between rainfall rate and radar reflectivity in the measurement of precipitation", J. Appl. Meteor., vol. 7, pp. 465-474, 1968.

(3) W. Hitschfeld and J. Bordan, "Errors inherent in the radar measurement of rainfall at attenuating wavelengths", J. Meteor., vol. 11, pp. 58-67, 1954.

(4) P. J. Eccles and E. A. Mueller, "X-band attenuation and liquid water content estimation by a dual-wavelength radar", J. Appl. Meteor., vol. 10, pp. 1252-1259, 1971.

(5) C. W. Ulbrich and D. Atlas, "The use of radar reflectivity and microwave attenuation to obtain improved measurements of precipitation parameters", Preprints 16th Radar Meteor. Conf., Amer. Meteor. Soc., Boston, pp. 496-503, 1975.

(6) J. Goldhirsh and I. Katz, "Estimation of rain drop size distribution using multiple wavelength radar systems", Radio Science, vol. 9, pp. 439-446, 1974.

(7) T. A. Seliga and V. N. Bringi, "Potential use of radar differential reflectivity measurements at orthogonal polarizations for measuring precipitation", J. Appl. Meteor., vol. 15, pp. 69-76, 1976.

(8) S. M. Cherry, J. W. F. Goddard and M. P. M. Hall, "Examination of rain drop sizes using a dual-polarization radar", Preprints 19th Radar Meteor. Conf., Amer. Meteor. Soc., Boston, pp. 526-531, 1980.

(9) D. B. Hodge and G. L. Austin, "The comparison between radar- and radiometer-derived rain attenuation for earth-space links", Radio Science, vol. 12, pp. 733-740, 1977.

(10) R. T. H. Collis and M. G. H. Ligda, "A radar raingage", Proc. 9th Radar Conf., Amer. Meteor. Soc., Boston, pp. 391-395, 1961.

(11) R. T. H. Collis, "Radar precipitation measurements", Proc. 11th Radio Meteor. Conf., Amer. Meteor. Soc., Boston, pp. 142-145, 1964.

(12) R. Juillerat and S. Godard, "Etude de la correlation entre l'attenuation atmospherique d'une onde E.M. et l'intensite de pluie." Internal company report, Lignes Telegraphiques et Telephoniques, Paris, April 17, 1963.

(13) T. W. Harrold, "The attenuation of 8.6 mm wavelength radiation in rain", Proc. Inst. Elec. Eng. (London), vol. 114, pp. 201-203, 1967.

(14) D. Atlas and C. W. Ulbrich, "Path and area-integrated rainfall measurements by microwave attenuation in the 1-3 cm band", Preprints 17th Radar Meteor. Conf., Amer. Meteor. Soc., Boston, pp. 406-413, 1976.

(15) J. Eckerman, R. Meneghini and D. Atlas, "Average rainfall determination from a scanning beam spaceborne radar", NASA Tech. Memo., 79664, Nov. 1978.

(16) J. F. A. Ormsby, "Some results on attenuation compensation analysis", Preprints 15th Radar Meteor. Conf., Amer. Meteor. Soc., Boston, pp. 144-148, 1972.

(17) R. Meneghini, "Rain rate estimates for an attenuating radar", Radio Science, vol. 13, pp. 459-470, 1978.

(18) J. S. Marshall and W. Hitschfeld, "Interpretation of the fluctuating echo from randomly distributed scatterers, Part 1", Can. J. Phys., vol. 31, pp. 962-994, 1953.

(19) A. Stogyrn, "Error analysis of the Goldhirsh-Katz method of rainfall determination by the use of a two frequency radar", Reprt 1833 TR-4, Aerojet Electrosystems Co., Azusa, CA., 1975.

(20) R. M. Lhermitte, "Weather echos in Doppler and conventional radars", Preprints 10th Radar Meteor. Conf., Amer. Meteor. Soc., Boston, pp. 323-329, 1963.

(21) G. L. Austin and R. W. Fetter, "Pulse compression for meteorological radar", Science Rep. MW-70, Stormy Weather Group, McGill Univ., Montreal, Can., Jan. 1972.

(22) P. R. Krehbiel and M. Brook, "A broad-band noise technique for fast-scanning radar observations of clouds and clutter targets", IEEE Trans. Geo. Elect., GE-17, pp. 196-204, 1979.

(23) F. T. Ulaby, "Vegetation Clutter Model", IEEE Trans. Ant. and Propag., AP-28, pp. 538-545, 1980.

(24) M. Schaffner, R. Rinehart, and R. Leonardi, "Detection of nonuniformities within the radar measurement cell", Preprints 19th Radar Meteor. Conf., Amer. Meteor. Soc., Boston, pp. 256-263, 1980.

## APPENDIX

## AVERAGE RADAR RETURN FROM THE RAIN AND GROUND

In the text, the explicit forms of the mean return power from the rain and the surface are not given. We wish here to write down these expressions and indicate how they may be simplified under certain conditions. We begin with an equation for the return power as a function of time, t, from an ensemble of scatterers. A slight generalization of the equation given in [1] can be made by keeping the attenuation factor inside the integral, i.e.,

$$P_R(t) = \frac{1}{(4\pi)^3} \int_r \int_\Omega \frac{\lambda^2 P_T(t - 2r/c)}{r^2} \eta G^2 e^{-0.46 \int_{S_1}^{S_2} k(s)\, ds} \, dr\, d\Omega \tag{A1}$$

where $\eta$ is the reflectivity, $P_T$ is the transmitted power, r is the range measured from the radar, $\lambda$ is the radar wavelength and G is the antenna gain function. We choose spherical coordinates (r, $\theta$, $\phi$) with respect to an origin located on the radar at an altitude $z_o$ above the ground. The polar angle $\theta$ is measured with respect to the z axis which points in the nadir direction. As in the text, k(s) is the attenuation coefficient in db/km. In general, $\eta$, $S_1$, $S_2$ are functions of (r, $\theta$, $\phi$) because of the finite extent of the region of precipitation. The antenna gain function G is taken to be rotationally symmetric about the direction of maximum gain, $\theta = \theta_N$, $\phi = 0$, so that,

$$G(\phi,\theta) = \tilde{G}(\psi)$$

where $\psi$ is the angle between the vectors (r sin $\theta_n$, 0, r cos $\theta_n$) and (r cos $\phi$ sin $\theta$, r sin $\phi$ sin $\theta$, r cos $\theta$) and is given by

$$\psi = \cos^{-1} (\cos\phi \sin\theta \sin\theta_N + \cos\theta \cos\theta_N)$$

To simplify (A1) we make the following assumptions: we choose a uniform rain rate from the ground up to an altitude $z_s$. We further assume a rectangular transmitted pulse of duration $\tau$; the return power is then sampled at times $t_j = 2r_j/c + \tau$, j = 1, ..., n where $r_{j+1} - r_j = h = c\tau/2$. The quantity, $P_R$ $(t = 2r_j/c+\tau)$, is the return power from the rain at the jth range bin which we denote by $P_{R_j}$. The final approximation is to neglect the rain return from all but the main lobe. Equation (A1) becomes

$$P_{R_j} = \frac{P_T \lambda^2 \eta}{(4\pi)^3} \int_{r_j}^{r_j+h} \int_{4\pi} \frac{G_m^2(\phi,\theta)\, F(r,\phi,\theta)}{r^2} e^{-0.46\, k \int_{s_1}^{s_2} ds} dr\, d\Omega \qquad (A2)$$

where

$$G_m = \begin{cases} G & \text{within main lobe} \\ 0 & \text{elsewhere} \end{cases}$$

and F is a fill factor, being unity for that region of the range bin which intercepts the rain and zero elsewhere. For a fixed $\theta$, $s_1 = (z_o - z_s)\sec\theta$, $s_2 = r$ so that $s_2 - s_1$ is simply the distance through the storm to range r at a particular value of $\theta$. Using the relation $\eta = \pi^5 |K|^2 Z/\lambda^4$ [2], then

$$P_{R_j} = C Z \int_{4\pi} \int_{r_j}^{r_j+h} \frac{G_m^2(\phi,\theta)\, F(r,\phi,\theta)}{r^2} e^{-0.46\,(r - \Delta\sec\theta)} dr\, d\Omega \qquad (A3)$$

where,

$C = \pi^2 |K|^2 P_T/64\lambda^2$

$\Delta = (z_o - z_s)$

$|K|^2 = |m^2 + 2|/|m^2 - 1|$

m = complex index of refraction of water

The r integration in (A3) can be done for an arbitrary range bin; this results, however, in three different expressions for $P_{R_j}$ depending on whether the bin is partially filled at the storm top or at the ground cell of whether the cell is fully filled. To be brief, we write down $P_{R_j}$ only for a bin filled with rain. The remaining cases can be done in a similar manner except that greater care is needed in specifying the $\theta$ limits of integration.

For a fully filled bin, F = 1. Integrating by parts, then

$$\int_{r_j}^{r_j+h} \frac{e^{-\gamma r}}{r^2} dr = \left( \frac{e^{-\gamma r_j}}{r_j} - \frac{e^{-\gamma(r_j+h)}}{(r_j+h)} \right) + \gamma \left( E_1(\gamma(r_j+h)) - E_1(\gamma r_j) \right)$$

where,

$$E_1(x) = \int_x^\infty \frac{e^{-t}}{t}\, dt$$

$$\gamma = 0.46\,\alpha$$

Assuming that $\gamma r_j >> 1$, we can use a large argument expansion on $E_1(x)$ [3]. Omitting $\vartheta(r_j^{-3})$ terms then

$$\int_{r_j}^{r_j+h} \frac{e^{-\gamma t}}{t^2}\, dt \approx \frac{1}{\gamma r_j^2}\, e^{-\gamma r_j} \left(1 - e^{-\gamma h}\, r_j^2/(r_j + h)^2\right)$$

The return power from a uniformly filled range bin then becomes

$$P_{R_j} \approx \frac{CZ}{\gamma r_j^2} \left(1 - \frac{e^{-\gamma h}\, r_j^2}{(r_j+h)^2}\right) \int_{4\pi} G_m^{\,2}(\phi,\theta)\, e^{-\gamma(r_j - \Delta \sec\theta)}\, d\Omega \ . \qquad \text{(A4)}$$

If the attenuation per range bin is small, i.e. $\gamma h << 1$, and $r_j >> h$ then

$$\gamma^{-1} \left(1 - e^{-\gamma h}\, (r_j/(r_j + h))^2\right) \approx h$$

Furthermore, if the main beam is sufficiently narrow so that $\sec\theta \approx \sec\theta_N$ where $\theta_N$ is the angle between nadir and the direction of maximum gain, then

$$P_{R_j} \approx \frac{C_R Z}{r_j^2}\, e^{-\gamma(r_j - \Delta \sec\theta_N)} \qquad \text{(A5)}$$

where

$$C_r = \frac{h\,\pi^3\,|K|^2\,P_T}{32\,\lambda^2} \int_0^{\theta_B/2} \tilde{G}^2(\psi) \sin\psi\, d\psi \qquad \text{(A6)}$$

having used the fact that

$$\int_{4\pi} G_m^{\,2}(\phi,\theta)\, d\Omega = 2\pi \int_0^{\theta_B/2} \tilde{G}^2(\psi) \sin\psi\, d\psi \ .$$

where $\theta_B$ is the angular extent of the main lobe. Thus, (A6), for a symmetric antenna pattern, involves only a single integration over $\psi$.

For the purpose of the simulation in the text, the mean return power has been generated using (A4) (and the corresponding expressions at the storm top and bottom where the beam is partially filled) instead of (A5) since the assumptions $\gamma h \ll 1$, $\sec\theta \approx \sec\theta_N$ are not always valid for the frequencies and beamwidths that we wish to consider.

For a nonuniform rain rate, the r integration can not be done so that a volume integration is necessary for finding $P_{R_j}$. If the main beam is sufficiently narrow, however, and $\gamma h \ll 1$, then we have, approximately, for a filled range bin

$$P_{R_j} = \frac{C_R\, Z_j}{r_j^2}\, A_j \tag{A7}$$

where $A_j$ is the attenuation factor given by,

$$A_j = e^{-0.46\, h \sum_{i=1}^{j} \epsilon_i\, k_i} \tag{A8}$$

and $C_R$ is given by (A6). Defining the measured reflectivity factor by $Z_{m_j} = Z_j\, A_j$ then (A7) becomes

$$P_{R_j} = C_R\, Z_{m_j}/r_j^2 \tag{A9}$$

To obtain the backscattered power from the surface, we begin with the expression (1),

$$P_G'(t) = \frac{\lambda^2}{(4\pi)^3} \int \frac{P_T(t - 2r/c)\, G^2\, \sigma^\circ(\phi,\theta)}{r^4}\, e^{-0.46 \int_{s_1}^{s_2} k(s)\, ds}\, dS' \tag{A10}$$

where the region of integration is over the entire ground plane. We again assume a rectangular pulse of duration $\tau$ and sample the return waveform at times $t_j = 2r_j/c + \tau$, $j = 1, \ldots, n$. The notation $P_G(t_j = 2r_j/c + \tau) = P_{G_j}$ is used. Assuming that $h \ll r_j\, \theta_B$, where $\theta_B$ is the angular extent of the main lobe, then $\theta$ varies only slightly over the region of integration. This implies that the attenuation is essentially constant over the area of integration so that it can be taken outside the integral. If we furthermore assume that $\sigma^\circ$ is independent of $\phi$ then $\sigma^\circ(\phi,\theta) \approx \sigma^\circ(\theta_M)$, where $\theta_M$ is defined below. Under these assumptions, the return power from the surface, in the presence of

precipitation, is

$$P'_{G_j} = \frac{\lambda^2 P_T \sigma^o(\theta_m) A_j}{(4\pi)^3} \int_{\phi=0}^{2\pi} \int_{\rho=\rho_a}^{\rho_b} \frac{G^2(\theta_m,\phi)}{(z_o^2+\rho^2)^2} \rho \, d\rho \, d\phi$$

where $A_j$ is given by (A8) and

$$\rho_a = (r_j^2 - z_o^2)^{1/2}$$

$$\rho_b = ((r_j + h)^2 - z_o^2)^{1/2}$$

Performing the $\rho$ integration and using the approximation

$$\frac{1}{r_j^2} - \frac{1}{(r_j+h)^2} = 2h/r_j^3$$

which is suitable for $r_j >> h$, then

$$P'_{G_j} = C_G \sigma^o(\theta_M) A_j / r_j^3 \qquad \text{(A11)}$$

where

$$\theta_M = \mathrm{Tan}^{-1}((\rho_a + \rho_b)/2z_o) \qquad \text{(A12)}$$

$$C_G = (\lambda^2 P_T h/(4\eta)^3) \int_0^{2\pi} G^2(\theta_M,\phi) \, d\phi \qquad \text{(A13)}$$

The calculation of the return power from the surface in the absence of precipitation, $P_{G_j}$, follows at once from (A11) by setting $A_j$ equal to unity, i.e.,

$$P_{G_j} = C_G \sigma^o(\theta_M)/r_j^3$$

We now wish to indicate how $Z_{m_j}$ can be found in terms of measurable quantities. From (A9),

$$Z_{m_j} = r_j^2 P_{R_j}/C_R \qquad \text{(A14)}$$

where $P_{R_j}$ is the rain return power from the jth range bin. Implicit in the choice of calibration constant $C_R$ is the assumption of a fully filled range bin. If the extent of the beamfilling were known, $C_R$, could be replaced by a calibration constant which takes this into account. However,

we assume that no such apriori knowledge is available. Thus, the offset errors of $Z_{m_j}$ in (A14) arise from partial filling of the range bin, the normal calibration errors in $C_R$, and the additional errors introduced by the approximations that led to (A9). Noticing, moreover, that $P_{1_j}$ rather than $P_{R_j}$ is a measured quantity, (A14) must be changed to

$$Z_{m_j} = r_j^2 \, P_{1_j}/C_R \tag{A15}$$

where from equation (5) of the text,

$$P_{1_j} = P_{R_j} + P_{G_j} + P_{N_1} \; . \tag{A16}$$

The terms of $P_{1_j}$, other than $P_{R_j}$, are seen to introduce an additional offset into $Z_{m_j}$. For the purposes of the simulation presented in the text, the $Z_{m_j}$, j = 1, ..., n that appear in the rain rate estimates are generated by means of (A15) and (A16). The mean value of $P'_{G_j}$ is found from (A11) through (A13); the mean of $P_{R_j}$, for a range bin uniformly filled with rain, is found from (A4).

## REFERENCES

(1) M. I. Skolnik, Ed., Radar Handbook. McGraw-Hill, 1970, pp. 24-29, 25-2.

(2) L. J. Battan, Radar Observations of the Atmosphere, University of Chicago Press, 1973, p. 44.

(3) M. Abramowitz and I. A. Stegun, Handbook of Mathematical Functions, National Bureau of Standards, 1972, p. 231.

Table 1

| | | |
|---|---|---|
| $P_T$ | = | peak transmit power = 1 kw |
| h | = | range resolution = 0.3 km |
| $D/\lambda$ | = | antenna diameter to wavelength ratio = 300 |
| $G(\theta)$ | = | antenna gain = $\dfrac{4\pi \mid E_i(\theta) \mid^2}{\int \mid E_i(\theta) \mid^2 d\Omega}$ |
| $E_i(\theta)$ | = | incident electric field = $J_1(\pi D \sin\theta/\lambda)/(D \sin\theta/\lambda)$ |
| $g(\rho)$ | = | antenna aperture illumination = 1 ($o \leq \rho \leq D/2$) |
| PRF | = | pulse repitition frequency = 10 kHz |
| m | = | number of multiple beams = 4 |
| $z_o$ | = | storm height = 5 km |
| $z_s$ | = | satellite altitude = 700 km |
| $V_s$ | = | satellite velocity = 7 km/sec |

Table 2

| Wavelength (cm) | $S_o$ (db) | Min R (mm/hr) | Max R (mm/hr) |
|---|---|---|---|
| 0.86 | 0 | <1 | 12 |
| | 0.9 | 2 | |
| | 1.8 | 3.5 | |
| | 2.7 | 5 | |
| 1.24 | 0 | <1 | 25 |
| | 0.9 | 4 | |
| | 1.8 | 6 | |
| | 2.7 | 8 | |
| 1.87 | 0 | 1 | 55 |
| | 0.9 | 8 | |
| | 1.8 | 14 | |
| | 2.7 | 20 | |

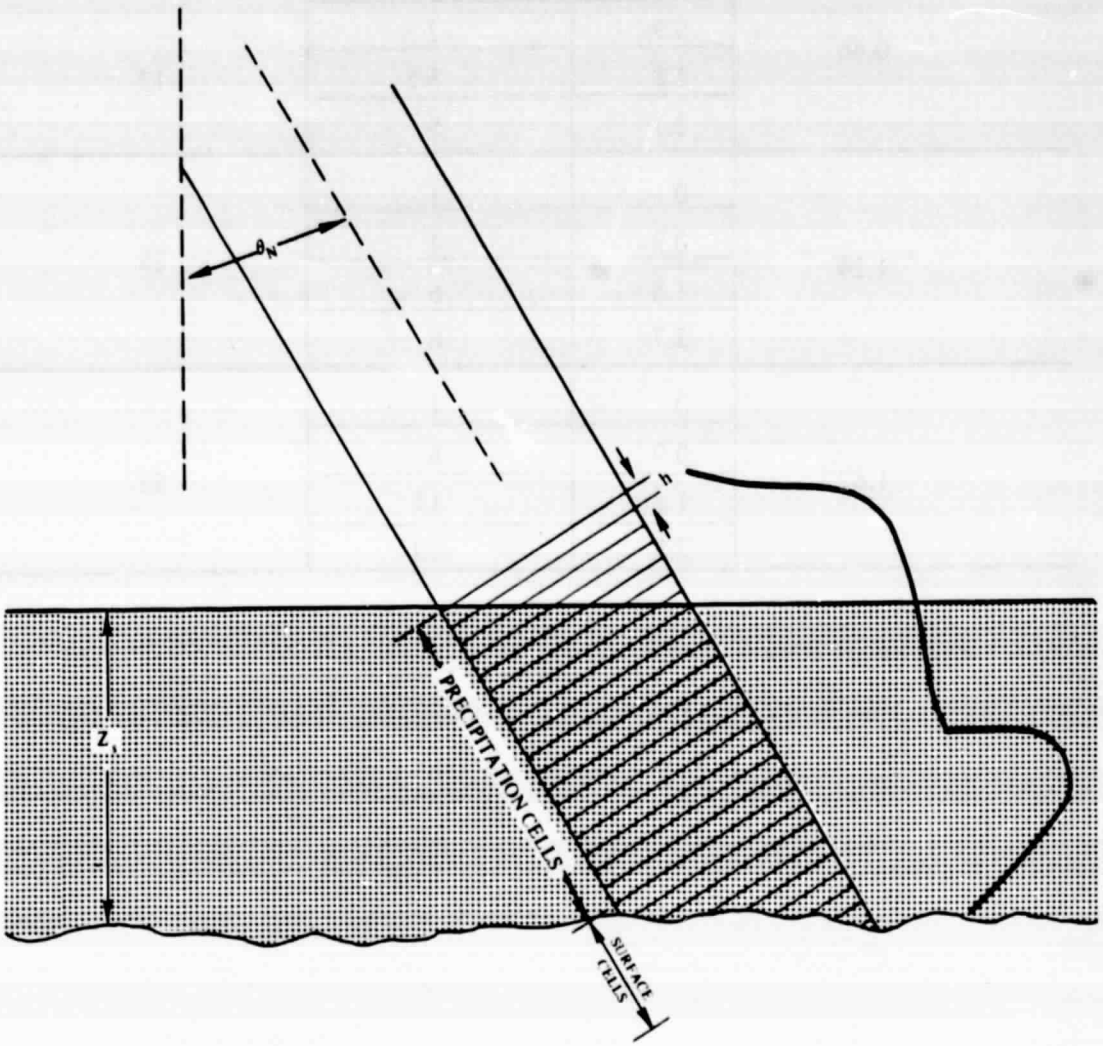


Figure 1. Spaceborne Radar Geometry

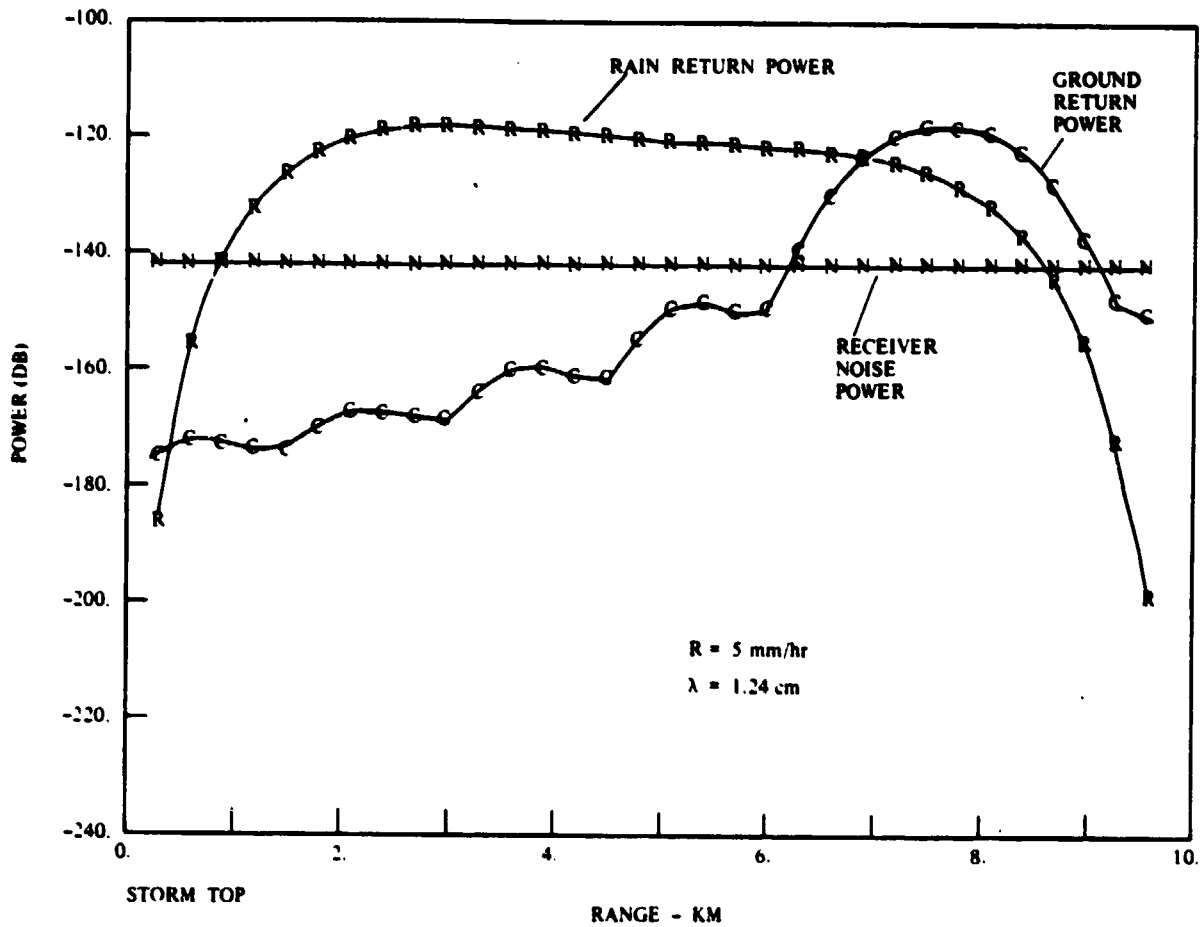
-100.
-120.
-140.
-160.
-180.
-200.
-220.
-240.
POWER (DB)
RAIN RETURN POWER
GROUND RETURN POWER
RECEIVER NOISE POWER
R = 5 mm/hr
λ = 1.24 cm
0.
2.
4.
6.
8.
10.
STORM TOP
RANGE - KM

Figure 2

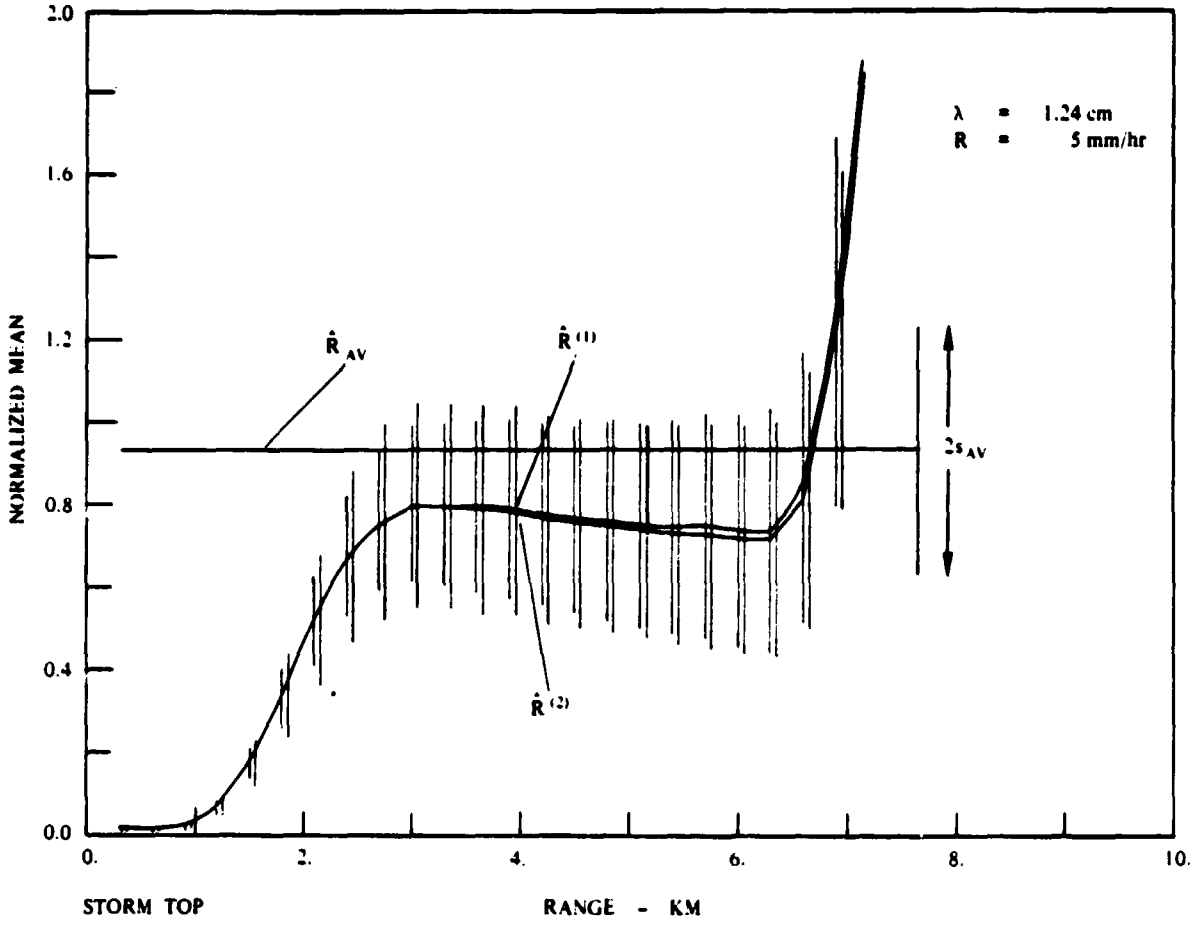
2.0
1.6
1.2
0.8
0.4
0.0
NORMALIZED MEAN
λ = 1.24 cm
R = 5 mm/hr
$\hat{R}_{AV}$
$\hat{R}^{(1)}$
$\hat{R}^{(2)}$
$2s_{AV}$
0.
2.
4.
6.
8.
10.
STORM TOP
RANGE - KM

Figure 3

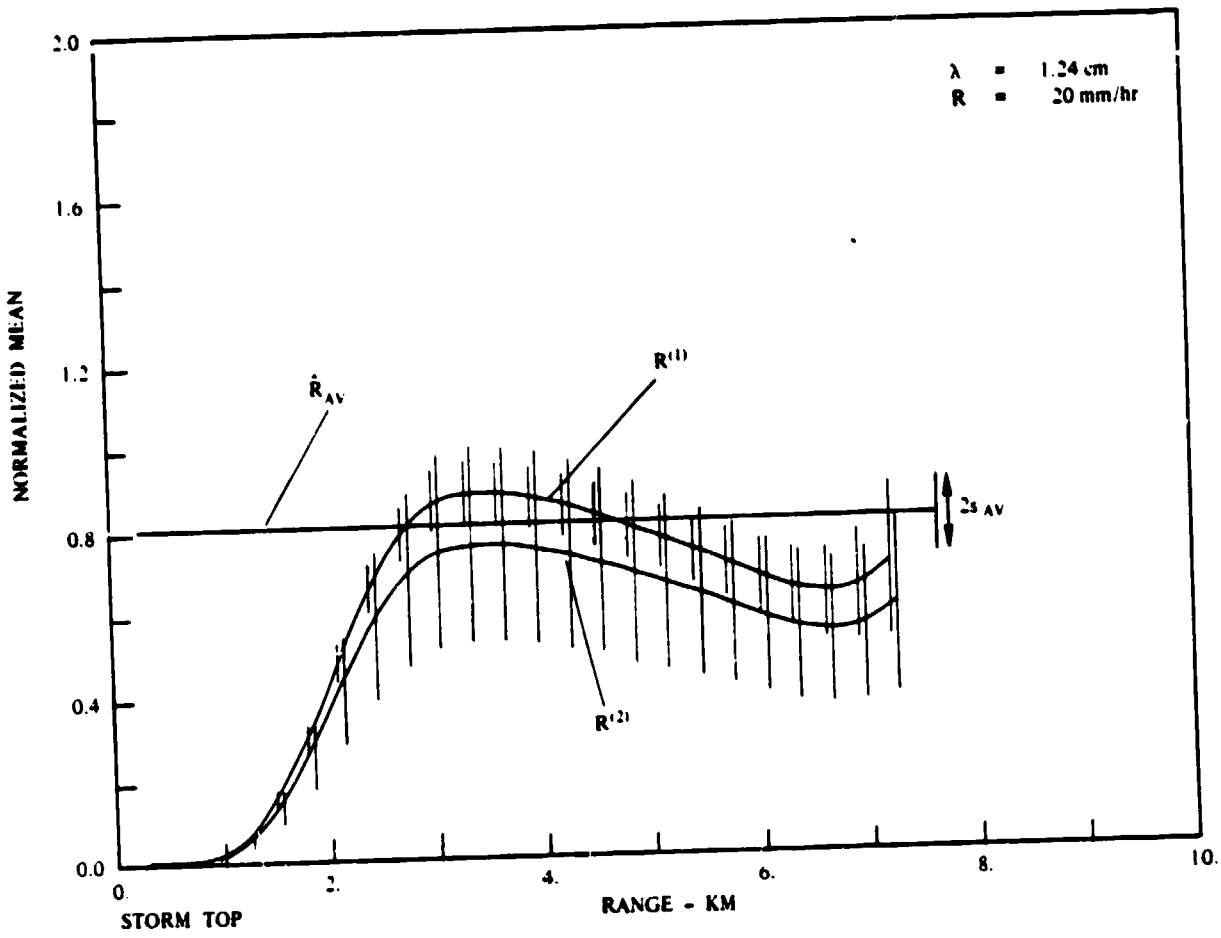
λ = 1.24 cm
R = 20 mm/hr
NORMALIZED MEAN
2.0
1.6
1.2
0.8
0.4
0.0
$\hat{R}_{AV}$
$R^{(1)}$
$2s_{AV}$
$R^{(2)}$
0.
2.
4.
6.
8.
10.
STORM TOP
RANGE - KM

Figure 4

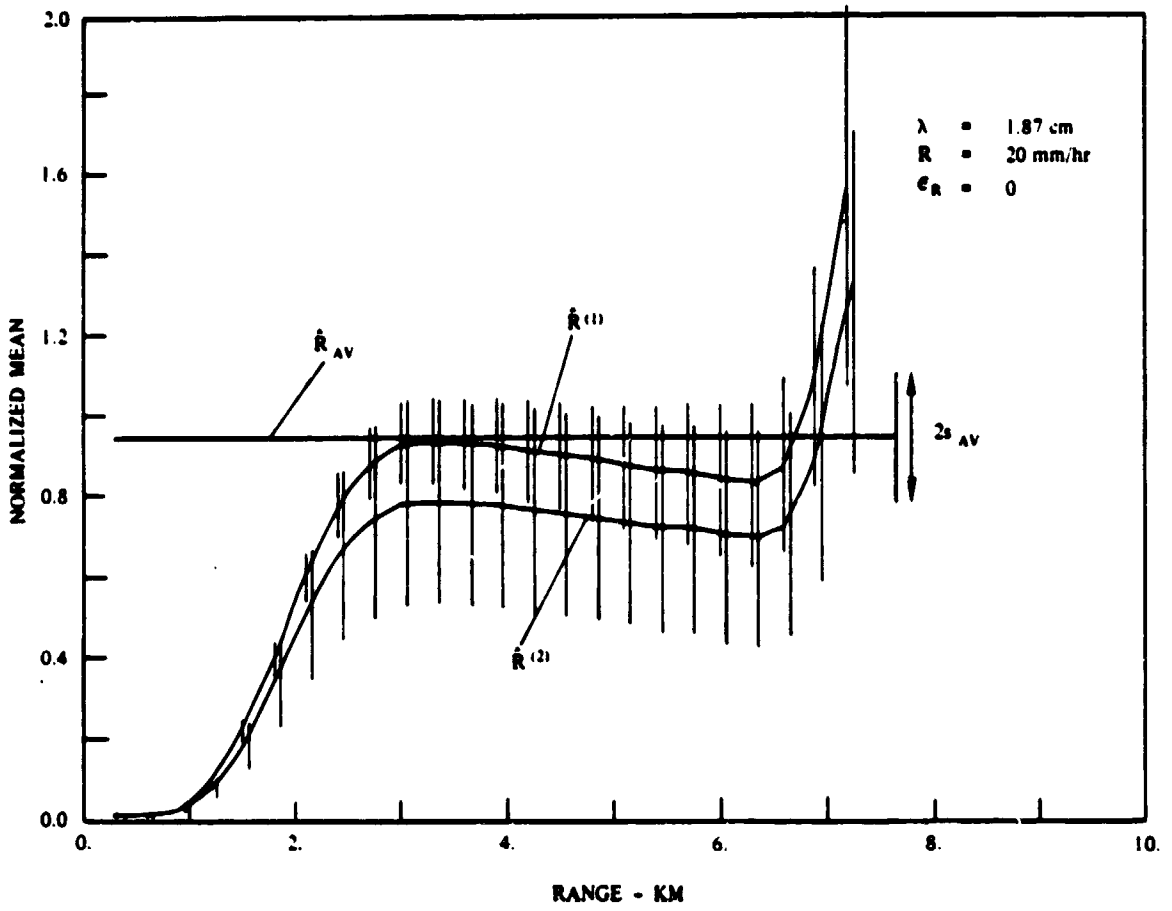
2.0
1.6
1.2
0.8
0.4
0.0
NORMALIZED MEAN
0.
2.
4.
6.
8.
10.
RANGE - KM
λ = 1.87 cm
R = 20 mm/hr
$\epsilon_R$ = 0
$\hat{R}_{AV}$
$\hat{R}^{(1)}$
$\hat{R}^{(2)}$
$2s_{AV}$

Figure 5

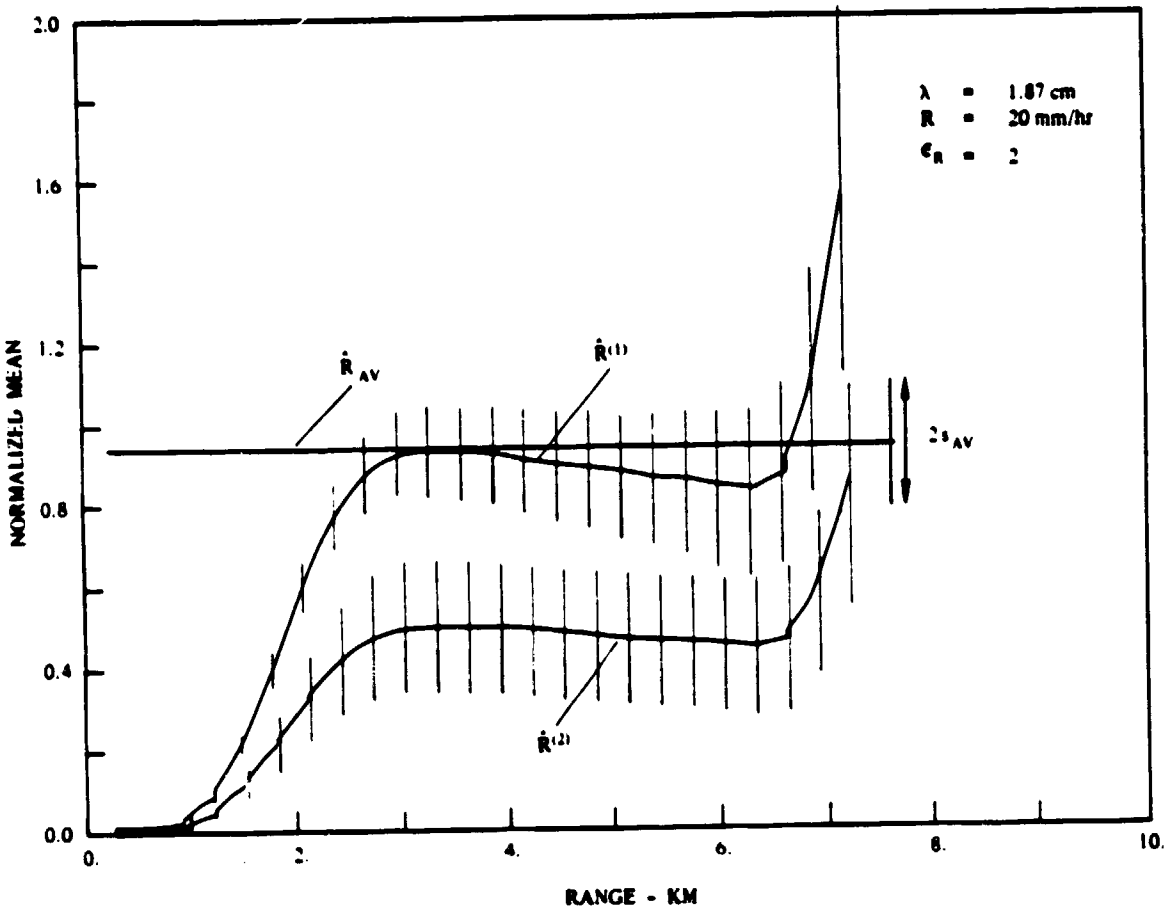
2.0
1.6
1.2
0.8
0.4
0.0
NORMALIZED MEAN
0.
2.
4.
6.
8.
10.
RANGE - KM
λ = 1.87 cm
R = 20 mm/hr
$\epsilon_R$ = 2
$\hat{R}_{AV}$
$\hat{R}^{(1)}$
$\hat{R}^{(2)}$
$2s_{AV}$

Figure 6